



## The C<sub>32</sub> alkane-1,15-diol as a proxy of late Quaternary riverine input in coastal margins

Julie Lattaud<sup>1\*</sup>, Denise Dorhout<sup>1</sup>, Hartmut Schulz<sup>2</sup>, Isla S. Castañeda<sup>1,4</sup>, Jaap S. Sinninghe

Damsté<sup>1,3</sup>, Stefan Schouten<sup>1,3</sup>

<sup>1</sup>*NIOZ Royal Netherlands Institute for Sea Research, Department of Marine Microbiology and Biogeochemistry, and Utrecht University, The Netherlands*

<sup>2</sup>*University of Tübingen, Department of Geosciences, Hölderlinstraße 12, D-72074 Tübingen, Germany*

<sup>3</sup>*Utrecht University, Department of Earth Sciences, Faculty of Geosciences, Budapestlaan 4, 3584 CD Utrecht, The Netherlands.*

<sup>4</sup>*Present address: University of Massachusetts, Department of Geological sciences, 244 Morrill Science Center, Amherst, United States of America*

\*Corresponding author: Julie.lattaud@nioz.nl



1 ABSTRACT

2 The study of past sedimentary records from coastal margins allows us to reconstruct variations  
3 of terrestrial input into the marine realm and to gain insight into continental climatic variability.  
4 There are numerous organic proxies for tracing terrestrial input into marine environments but  
5 none that strictly reflect riverine organic matter input. Here, we test the fractional abundance of  
6 the C<sub>32</sub> alkane 1,15-diol relative to all 1,13- and 1,15-diols ( $F_{1,15-C32}$ ) as a tracer of riverine input  
7 in the marine realm in surface and Quaternary (0–45 ka) sediments on the shelf off the Zambezi  
8 and nearby smaller rivers in the Mozambique Channel (western Indian Ocean). A Quaternary (0–  
9 22 ka) sediment record off the Nile River mouth in the Eastern Mediterranean was also studied  
10 for diols. For the Mozambique Channel, surface sediments of sites most proximal to  
11 Mozambique rivers showed the highest  $F_{1,15-C32}$  (up to 10%). The sedimentary record shows high  
12 (15–35%) pre-Holocene  $F_{1,15-C32}$  and low (<10%) Holocene  $F_{1,15-C32}$  values, with a major decrease  
13 between 18 and 12 ka.  $F_{1,15-C32}$  is significantly correlated ( $r^2=0.83$ ,  $p<0.001$ ) with the BIT index, a  
14 proxy for soil and riverine input, which declines from 0.25–0.60 for the pre-Holocene to <0.10  
15 for the Holocene. This decrease of both  $F_{1,15-C32}$  and the BIT is interpreted to be mainly due to an  
16 increasing sea level, which caused the Zambezi River mouth to become more distal to our study  
17 site, thereby decreasing riverine input at the core location. Some small discrepancies are  
18 observed between the records of the BIT index and  $F_{1,15-C32}$  for Heinrich Event 1 (H1) and  
19 Younger Dryas (YD), which can be explained by a change in soil sources in the catchment area  
20 rather than a change in river influx. Like for the Mozambique Channel, a significant correlation  
21 between  $F_{1,15-C32}$  and the BIT index ( $r^2=0.38$ ,  $p<0.001$ ) is observed for Eastern Mediterranean  
22 Nile record. Here also, the BIT index and  $F_{1,15-C32}$  are lower in the Holocene than in the pre-



23 Holocene, which is likely due to the sea level rise. In general, the differences between BIT index  
24 and F<sub>1,15-c32</sub> Eastern Mediterranean Nile records can be explained by the fact that the BIT index  
25 is not only affected by riverine runoff but also by vegetation cover with increasing cover leading  
26 to lower soil erosion. Our results confirm that F<sub>1,15-c32</sub> is a complementary proxy for tracing  
27 riverine input of organic matter into marine shelf settings and, in comparison with other  
28 proxies, it seems not to be affected by soil and vegetation changes in the catchment area.

29



30

31 **1. Introduction**

32 Freshwater discharge from river basins into the ocean has an important influence on the  
33 dynamics of many coastal regions. Terrestrial organic matter (OM) input by fluvial and aeolian

34 transport represents a large source of OM to the ocean (Schlesinger and Melack, 1981). Deltaic

35 and marine sediments close to the outflow of large rivers form a sink of terrestrial OM and

36 integrate a history of river, catchment, and oceanic variability (Hedges et al, 1997).

37 Terrestrial OM can be differentiated from marine OM using carbon to nitrogen (C/N) ratios and

38 the bulk carbon isotopic composition ( $^{13}\text{C}$ ) of sedimentary OM (e.g. Meyers, 1994). The

39 abundance of N-free macromolecules such as lignin or cellulose result in organic carbon-rich

40 plant tissues that lead to an overall higher C/N ratio for terrestrial OM compared to aquatic

41 organisms (Hedges et al., 1986). However, this ratio may be biased when plant-tissues gain

42 nitrogen during bacterial degradation and when planktonic OM preferentially lose nitrogen over

43 carbon during decay (Hedges and Oades, 1997). Differences in the stable carbon isotopic

44 composition may also be used to examine terrestrial input as terrestrial OM is typically depleted

45 in  $^{13}\text{C}$  ( $\delta^{13}\text{C}$  of -28 to -25‰) compared to marine OM (-22 to -19‰). However, C<sub>4</sub> plants have

46  $\delta^{13}\text{C}$  values of around -12‰ (Fry et Sherr, 1984 ; Collister et al. 1994; Rommerskirchen et al.,

47 2006) and thus a substantial C<sub>4</sub> plant contribution can make it difficult to estimate the

48 proportion of terrestrial to marine OM in certain settings (Goñi et al., 1997).

49 Biomarkers of terrestrial higher plants are also used to trace terrestrial OM input into marine

50 sediments. For example, plant leaf waxes such as long-chain *n*-alkanes are transported and

51 preserved in sediments (Eglinton and Eglinton 2008, and references cited therein) and can



52 provide information on catchment integrated vegetation or precipitation changes (e.g. Ponton  
53 et al., 2014), while soil specific bacteriohopanepolyols (BHP) are biomarkers of soil bacteria and  
54 indicate changes in soil transport (Cooke et al., 2008). Similarly, branched glycerol dialkyl  
55 glycerol tetraethers (brGDGTs) are widespread and abundant in soils (Weijer et al., 2007, 2009)  
56 and can be used to trace soil OM input into marine settings via the branched and isoprenoid  
57 tetraether (BIT) Index (Hopmans et al., 2004). However, brGDGTs can also be produced in-situ in  
58 rivers (De Jonge et al., 2015) and thus the BIT index does not reflect soil OM input only.  
59 Moreover, because the BIT index is the ratio of brGDGTs to crenarchaeol (an isoprenoidal GDGT  
60 predominantly produced by marine Thaumarchaeota; Sinninghe Damsté et al., 2002), the BIT  
61 index can also reflect changes in marine OM productivity instead of changes in terrestrial OM  
62 input in areas where primary productivity is highly variable, i.e. where the quantity of  
63 crenarchaeol is variable (Smith et al., 2012).  
64 Although these terrestrial organic proxies are useful to trace soil, river or vegetation input into  
65 marine sediments thus far there are no organic geochemical proxies to specifically trace riverine  
66 OM input. However, recently, the C<sub>32</sub> 1,15-diol was proposed as a tracer for riverine OM input  
67 (De Bar et al., 2016; Lattaud et al., 2017). This diol, together with other 1,13 and 1,15-diols, are  
68 likely derived from freshwater eustigmatophyte algae (Volkman et al., 1999; Rampen et al.,  
69 2007, 2014b; Villanueva et al., 2014). Versteegh et al. (2000) showed that the proportion of C<sub>32</sub>  
70 1,15-diol to other diols was relatively higher closer to the mouth of the Congo River. Likewise,  
71 Rampen et al. (2012) observed that sediments from the estuarine Hudson Bay have a much  
72 higher proportion of C<sub>32</sub> 1,15-diol than open-marine sediments. More recent studies noted  
73 elevated amounts of the C<sub>32</sub> 1,15-diol in coastal sediments, and even higher amounts in rivers



74 indicating a continental source for this diol (De Bar et al., 2016, Lattaud et al., 2017). Since the  
75 C<sub>32</sub> 1,15-diol was not detected in soils distributed worldwide, production of this diol in rivers by  
76 freshwater eustigmatophytes is the most likely source of this compound which, therefore, can  
77 potentially be used as a proxy of riverine OM input to marine settings.  
78 Here we test the downcore application of this new proxy by analysing the fractional abundance  
79 of the C<sub>32</sub> 1,15-diol in a shelf sea record (0-45 ka) from the Mozambique Channel and a record  
80 (0-24 ka) from the Eastern Mediterranean Sea to reconstruct Holocene/Late Pleistocene  
81 changes in freshwater input of the Zambezi and Nile rivers, respectively. Analysis of surface  
82 sediments and comparison with previously published BIT index records (Castañeda et al., 2010;  
83 Kasper et al., 2015) allows us to assess the potential of the C<sub>32</sub> 1,15-diol as a tracer for riverine  
84 runoff in these coastal margins.

85

86 **2. Material and Methods**

87 **2.1. Study sites**

88 **2.1.1. Mozambique margin and Zambezi River**

89 The Mozambique Channel is located between the coasts of Mozambique and Madagascar  
90 between 11°S and 24°S and it plays an important role in the global oceanic circulation by  
91 transporting warm Indian Ocean surface waters into the Atlantic Ocean. The Zambezi River is  
92 the largest river that delivers freshwater and suspended particulate matter to the Mozambique  
93 Channel (Walford et al., 2005). The Zambezi River has a drainage area of 1.4 x 10<sup>6</sup> km<sup>2</sup> and an  
94 annual runoff between 50 and 220 km<sup>3</sup> (Fekete et al., 1999). It originates in northern Zambia,



95 flows through eastern Angola and Mozambique to reach the Indian Ocean. The Zambezi delta  
96 starts at Mopeia (Ronco et al., 2006) and the Zambezi plume enters the Mozambique Channel  
97 and flows northwards along the coast (Nehama and Reason, 2014). The rainy season in the  
98 catchment is in austral summer when the Intertropical convergence zone (ITCZ) is at its  
99 southernmost position (Beifuss and Santos, 2001; Gimeno et al., 2010; Nicholson et al., 2009).  
100 The seasonal variation of the Zambezi runoff varies between 7000 m<sup>3</sup>/s during the wet season  
101 to 2000 m<sup>3</sup>/s during the dry season (Beifuss and Santos, 2001). A few smaller Mozambique  
102 rivers other than the Zambezi River flow into the Mozambique Channel: the Ligonha, Licungo,  
103 Pungwe and Revue in Mozambique (together with the Zambezi River, they are collectively called  
104 "the Mozambique rivers" here).  
105 Past studies have shown that the deposition pattern of the Zambezi riverine detritus is variable  
106 with sea level, i.e. most of the time material was deposited downstream of the river mouth but  
107 during high sea level it was deposited northeast of the river mouth due to a shore current  
108 (Schulz et al., 2011). During the last glacial period the Zambezi riverine detritus followed a more  
109 channelized path (Schulz et al., 2011). Van der Lubbe et al. (2016) found that the relative  
110 influence of the Zambezi river compared to more northern rivers in the Mozambique Channel  
111 varied during Heinrich event 1 (H1) and the Younger Dryas (YD). Schefuss et al. (2011) studied  
112 the δ<sup>13</sup>C and δD of *n*-alkanes, and the elemental composition (Fe content) of core GeoB9307-3,  
113 located close to the present day river mouth (Fig. 1), and reported higher precipitation and  
114 riverine terrestrial input in the Mozambique Channel during the Younger Dryas and H1. This is in  
115 agreement with more recent results from Just et al. (2014) on core GeoB9307-3 and Wang et al.



116 (2013a) on core GIK16160-3, further away from the actual river mouth; both studies also  
117 showed an increased riverine terrestrial input during H1 and YD.

118

119 *2.1.2 Eastern Mediterranean Sea and Nile River*

120 The Eastern Mediterranean Sea is influenced by the input of the Nile River, which is the main  
121 riverine sediment supply with annual runoff of 91 km<sup>3</sup> and a sediment load of about 60 x 10<sup>9</sup>  
122 kg.yr<sup>-1</sup> (Foucault and Stanley, 1989; Weldeab et al., 2002). Offshore Israel, the Saharan eolian  
123 sediment supply is very low (Weldeab et al., 2002). A strong north-eastern current distributes  
124 the Nile River sediment along the Israeli coast toward our study site. The Nile River consists of  
125 two main branches: the Blue Nile (sourced at Lake Tana, Ethiopia) and the White Nile (sourced  
126 at Lake Victoria, Tanzania, Uganda). Precipitation in the Nile catchment fluctuates widely with  
127 latitude with the area north of 18°N dry most of the year and the wettest areas at the source of  
128 the Blue Nile and White Nile (Camberlin, 2009). This general distribution reflects the latitudinal  
129 movement of the ITCZ.

130 Castañeda et al. (2010) have shown that sea surface temperature (SST) (reconstructed with  
131 alkenones and TEX<sub>86</sub>) at the study site was following Northern Hemisphere climate variations  
132 with a cooling during the Last Glacial Maximum (LGM), Heinrich event 1 (H1) and Younger Dryas  
133 (YD) and warming during the early part of the deposition of sapropel 1 (S1). Associated with the  
134 cooling of H1 and the LGM, extreme aridity in the Nile catchment is observed as inferred from  
135 the δD of leaf waxes, in contrast to the time of Early Holocene S1 deposition, which corresponds  
136 to a more humid climate and enhanced Nile River runoff (Castañeda et al., 2016). Neodymium



137 ( $\varepsilon_{Nd}$ ) and strontium ( $^{87}\text{Sr}/^{88}\text{Sr}$ ) isotopes (Castañeda et al., 2016; Box et al., 2011, respectively)  
138 show an enhanced contribution of Blue Nile inputs when the climate is arid (H1, LGM) and an  
139 increased contribution of the White Nile when the climate is humid (S1). This change also affect  
140 the soil input into the Nile River, as inferred from the distribution of branched GDGTs, with a  
141 more arid climate reducing the vegetation in the Ethiopian highlands (source of the Blue Nile)  
142 and favoring soil erosion while during a more humid climate, vegetation increasing and soil  
143 erosion is less (Krom et al., 2002).

144 *2.2. Sampling and processing of the sediments*

145 *2.2.1. Mozambique Channel sediments*

146 We analyzed 36 core-top sediments (from multi cores) along a transect from the Mozambique  
147 coast to Madagascar coast (LOCO transect, Fallet et al. 2012). The LOCO core-tops have been  
148 previously studied by XRF and grain-size analysis (van der Lubbe et al., 2014, 2016) as well as for  
149 inorganic ( $\delta^{18}\text{O}$ , Mg/Ca) and organic (TEX<sub>86</sub>, UK'<sub>37</sub>) temperature proxies (Fallet et al., 2012). 25  
150 core-top sediments (from grabs, gravity or trigger-weight corers) retrieved during the R/V  
151 Valdivia's Expeditions VA02 (1971) and VA06 (1973) (called VA for the rest of this study, Schulz  
152 et al., 2011), comprising a north-south transect paralleling the East African coast, and spanning  
153 from 21°S to 15°N (Fig. 1a) were also analyzed. These surface sediments have been studied  
154 previously for element content (TOC, TON), isotopic content ( $\delta^{18}\text{O}$ ,  $\delta^{13}\text{C}$ ) as well as for mineral  
155 and fossil (foraminifera) content (Schulz et al., 2011). Piston core 64PE304-80 was obtained  
156 from 1329 m water depth during the INATEX cruise by the RV Pelagia in 2009 from a site  
157 (18°14.44'S, 37°52.14'E) located on the Mozambique coastal margin, approximately 200 km



158 north of the Zambezi delta (Fig. 1a). The age model of core 64PE304-80 is based on  $^{14}\text{C}$  dating of  
159 planktonic foraminifera (van der Lubbe, 2014; Kasper et al., 2015) and by correlation of log  
160 (Ti/Ca) data from XRF core scanning with those of nearby core GIK16160-3, which also has an  
161 age model based on  $^{14}\text{C}$  dating of a mixture of planktonic foraminifera (see van der Lubbe et al.,  
162 2014 for details).

163 The LOCO sediment core-tops were sliced into 0 - 0.25 and 0.25 - 0.5 cm slices and extracted as  
164 described by Fallet et al. (2012). Briefly, ultrasonic extraction was performed (x 4) with a solvent  
165 mixture of dichloromethane (DCM)/methanol (MeOH) (2 : 1 v/v). The total lipid extract (TLE)  
166 was then run through a  $\text{Na}_2\text{SiO}_4$  column to remove water. The 25 VA core-tops from the  
167 Valdivia's expedition were freeze dried on board and stored at 4 °C. They were extracted via  
168 Accelerator Solvent Extractor (ASE) using DCM: MeOH mixture 9:1 (v/v) and a pressure of 1000  
169 psi at 100 °C using three extraction cycles.

170 We analyzed sediments of core 64PE304-80 for diols using solvent extracts that were previously  
171 obtained for determination of the BIT index and  $\delta\text{D}$  ratio of alkenones (Kasper et al., 2015).  
172 Briefly, the core was sliced into 2 cm thick slices and the sediments were ASE extracted using  
173 the method described above.

174 For all Mozambique Channel sediments, the total lipid extract (TLEs) were separated through an  
175 alumina pipette column into three fractions: apolar (Hexane : DCM, 9:1 v/v), ketone (Hexane :  
176 DCM, 1:1 v/v) and polar (DCM : MeOH, 1:1 v/v). The polar fractions, containing the diols and  
177 GDGTs, were dissolved into a mixture of 99:1 (v/v) Hexane : Isopropanol and filtered through a  
178 0.45  $\mu\text{m}$  PTFE filters.



179    2.2.2. *Eastern Mediterranean sediment core*

180    Gravity core GeoB 7702-3 was collected during the R/V Meteor cruise M52/2 in 2002 from the  
181    slope offshore Israel (31°91.1'N, 34°04.4'E) at 562 m water depth (Castañeda et al., 2010). The  
182    chronology of this sedimentary record is based on 15 planktonic foraminiferal  $^{14}\text{C}$  AMS dates  
183    (Castañeda et al., 2010). The sediments have previously been analyzed for GDGTs, alkenones,  
184     $\delta\text{D}$  and  $\delta^{13}\text{C}$  of leaf wax lipids, and bulk elemental composition (Castañeda et al., 2010, 2016).  
185    Sediments were sampled every 5 cm and 1 cm thick, and previously extracted as described by  
186    Castañeda et al. (2010). Briefly, the freeze-dried sediment were ASE extracted and the TLEs  
187    were separated using an aluminum oxide column into 3 fractions as described above.

188    2.3. *Analysis of long-chain diols*

189    Diols were analyzed by silylation of the polar fraction with 10  $\mu\text{L}$  N,O-Bis(trimethylsilyl)-  
190    trifluoroacetamide (BSTFA) and 10  $\mu\text{L}$  pyridine, heated for 30 min at 60°C and adding 30  $\mu\text{L}$  of  
191    ethyl acetate. Diol analysis was performed using a gas chromatograph (Agilent 7990B GC)  
192    coupled to a mass spectrometer (Agilent 5977A MSD) (GC-MS) and equipped with a capillary  
193    silica column (25 m x 320  $\mu\text{m}$ ; 0.12  $\mu\text{m}$  film thickness). The oven temperature regime was as  
194    follows: held at 70 °C for 1 min, increased to 130 °C at 20 °C/min, increased to 320 °C at 4  
195    °C/min, held at 320 °C during 25 min. Flow was held constant at 2 mL/min. The MS source  
196    temperature was held at 250 °C and the MS quadrupole at 150 °C. The electron impact  
197    ionization energy of the source was 70 eV. The diols were quantified using selected ion  
198    monitoring (SIM) of ions m/z 299.4 ( $\text{C}_{28} 1,14$ ), 313.4 ( $\text{C}_{28} 1,13, \text{C}_{30} 1,15$ ), 327.4 ( $\text{C}_{30} 1,14$ ), and  
199    341.4 ( $\text{C}_{32} 1,15$ ) (Versteegh et al., 1997; Rampen et al., 2012).



200 The fractional abundance of the C<sub>32</sub> 1,15-diol is expressed as percentage of the total major diols  
201 as follows:

$$202 FC_{32\text{,}1,15} = \frac{[C_{32\text{,}1,15}]}{[C_{28\text{,}1,13}] + [C_{28\text{,}1,14}] + [C_{30\text{,}1,13}] + [C_{30\text{,}1,14}] + [C_{30\text{,}1,15}] + [C_{32\text{,}1,15}]} \times 100 \quad (1)$$

203

204 *2.4. Analysis of GDGTs*

205 GDGTs in the polar fractions of the extracts of the VA and LOCO core-top sediments were  
206 analyzed on an Agilent 1100 series LC/MSD SL following the method described by Hopmans et  
207 al. (2016). The BIT index was calculated according to Hopmans et al. (2004). We calculated the  
208 #ring tetra as described by Sinninghe Damsté et al. (2016) and the CBT index and soil pH as  
209 described by Peterse et al. (2012):

$$210 \#ring\ tetra = \frac{GDGT\ Ib + 2 \times GDGT\ Ic}{GDGT\ Ia + GDGT\ Ib + GDGT\ Ic} \quad (2)$$

$$211 CBT = \log\left(\frac{GDGT\ Ib + GDGT\ IIb}{GDGT\ Ia + GDGT\ IIa}\right) \quad (3)$$

$$212 pH = 7.9 - 1.97 \times CBT \quad (4)$$

213

214 **3. Results**

215 *3.1. Surface sediments of the Mozambique Channel*

216 F<sub>1,15-C32</sub> in surface sediments across the Mozambique Channel varies from 2.3 to 12.5% (Fig. 1d,  
217 1f) with one of the highest value in front of the Zambezi River mouth (10%). The core-tops  
218 located in front of other minor northern rivers (Licungo, Ligonha Rivers) are also characterized  
219 by values of F<sub>1,15-C32</sub> (>7.5%) higher than those further away from the coast (< 5%). The major



220 diol in all Mozambique surface sediments is the C<sub>30</sub> 1,15-diol (57.5±9.9%) with lower amounts of  
221 the C<sub>30</sub> 1,14-diol (21.1±6.0%) and C<sub>28</sub> 1,14-diol (13.2±4.9%) (Fig. 1f).

222 The values for the BIT index in surface sediments across the Mozambique Channel vary from  
223 0.01 to 0.42 (Fig. 1c). BIT values are highest in the most northern region (0.4) and in front of  
224 river mouths (0.2-0.3) compared to values found close to the coast of Madagascar (<0.04).

225 Following Sinninghe Damsté (2016), we calculated the #ring tetra (the relative abundance of  
226 cyclopentane rings in tetramethylated branched GDGTs) to determine if the brGDGTs are in-situ  
227 produced in the surface sediments or derived from the continent. The #ring tetra has an  
228 average of 0.39±0.03 with higher values in front of the river mouths (with the highest values  
229 close to the Madagascar rivers) and shows a clear decrease towards the open ocean (Fig. 1d).

230 The low #ring tetra indicate that there is likely limited in-situ sedimentary production of  
231 brGDGTs in the sediments of the Mozambique coastal shelf area except for the samples closest  
232 to the Madagascar coast where high #ring tetra values and low BIT values indicate in-situ  
233 production of brGDGTs. However, for the Mozambique shelf, the brGDGTs are mostly derived  
234 from the continent, confirming the use of the BIT index as a tracer for freshwater input in this  
235 region.

236 *3.2. Holocene and Late Quaternary sediments of the Mozambique Channel and Nile River*

237 In the sediments of the Mozambique Channel core 64PE304-80, F<sub>1,15-C32</sub> shows a wide range; it  
238 varies from 2.4 to 47.6% (Fig. 2). Between 44 and 39 ka the values are relatively stable (average  
239 of 27.6 ± 4.5%), then they rapidly decline between 39 and 36 ka to 11%. From this point on they  
240 gradually increase, reaching 37.4% at 17 ka. F<sub>1,15-C32</sub> is then rapidly decreasing until it reaches the



241 lowest values of the record after 12 ka (average of  $4.9 \pm 1.4\%$ ). Holocene sediments (0-11 ka)  
242 show relatively low and constant values of  $F_{1,15-C32}$  ( $5 \pm 1.5\%$ ), similar to the values found in the  
243 surface sediments of the area, i.e.  $3.5 \pm 1.6\%$  (Figs. 1 and 2d).  
  
244 The BIT index record shows similar changes (data from Kasper et al., 2014) as that of  $F_{1,15-C32}$ .  
245 Between 44 and 39 ka the average BIT value is  $0.43 \pm 0.06$ , then the BIT value decreases to 0.36  
246 at 36 ka, followed by an increase until 17 ka to reach 0.6, while the Holocene values are  
247 constant (average  $0.1 \pm 0.02$ ). The #ring tetra of branched GDGTs is constantly low (average  
248  $0.15 \pm 0.01$ ; Fig. S1a) between 44 to 15.5 ka, then increases to 0.4 at 8 ka and stays constant until  
249 the end of the Holocene (average  $0.34 \pm 0.03$ ). Overall, these values are low and do not approach  
250 the values (0.8-1.0) associated with in-situ production of branched GDGTs in coastal marine  
251 sediments (Sinninghe Damsté, 2016). The #ring tetra also shows a negative correlation with the  
252 BIT index throughout the record ( $R^2=0.74$ ,  $p<0.05$ ), indicating that when BIT values are high,  
253 #ring tetra is low. Therefore, high BIT values can definitely be associated with terrestrial brGDGT  
254 input. If we assume the in-situ production of brGDGTs in the river (e.g. DeJonge et al., 2015; Zell  
255 et al., 2015) is minimal, we can then infer sources of soils from the different catchment areas by  
256 reconstructing the soil pH via the CBT index (see equation 3 and 4, Peterse et al., 2012). This  
257 showed a constant soil pH (average  $6.2 \pm 0.1$ ) from 43 to 15 ka followed by a slight increase to 7  
258 at 8 ka and constant (average  $6.8 \pm 0.08$ ) at the end of Holocene (Fig. S1b).  
  
259 In Eastern Mediterranean sediment core GeoB 7702-3,  $F_{1,15-C32}$  ranges from 3.9 to 47.0%.  
260 Between 24 and 15 ka the values are slowly decreasing from 41% at 24 ka to 7% at 15 ka.  
261 Subsequently,  $F_{1,15-C32}$  raises sharply until 11.7 ka (44%) followed by a sharp decrease down to  
262 16% at 10 ka.  $F_{1,15-C32}$  increases again until 7.5 ka up to 30%, followed by a slow decrease in the



263 Late Holocene towards values as low as 6% (Fig. 3a). The BIT index (data from Castañeda et al.,  
264 2016) varies similar to F<sub>1,15-C32</sub>. It is constant between 24 and 17 ka (average 0.37±0.05), then  
265 decreases to 0.13 at 14.5 ka. It subsequently increases between 15.6 and 9 ka, before  
266 decreasing after 9 ka and stays constant in the Holocene (average 0.17±0.05). The #ring tetra of  
267 the brGDGTs (Fig. S1c) is constant from 24 to 15 ka (0.37±0.05) then shows lower values from 15  
268 to 7 ka (0.29±0.04) and, finally, increases again during the late Holocene (0.40±0.05). The BIT  
269 index and #ring tetra do not show a clear negative correlation as observed for the Mozambique  
270 core. However, the values of #ring tetra are well below 0.8-1.0, suggesting that in-situ  
271 production of brGDGTs does not play an important role, in line with the depth from which the  
272 core was obtained which is well below the zone of 100-300 m where in-situ production is most  
273 pronounced (Sinninghe Damsté, 2016). During parts of the record, low #ring tetra are associated  
274 with high BIT values, indicating that between 24 and 7 ka the brGDGT are mainly terrigenous.  
275 For the oldest part of the core, the soil pH shows a stable period from 24 to 14.8 ka (average  
276 6.94±0.07) then increases to 7.3 at 15 ka, followed by a large decrease (pH reaching 6.5 at 8.5  
277 ka). As the in-situ production of brGDGT is likely to be minimal in the latest part of the  
278 Holocene, the soil pH can be reconstructed via the CBT index and shows a stable pH (average of  
279 6.8±0.1).

280 **4. Discussion**

281 *4.1. Application of C<sub>32</sub> 1,15-diol as a proxy for riverine input in the Mozambique shelf.*  
282 The percentage of the C<sub>32</sub> 1,15-diol is overall relatively low (<10%) in the surface sediments of  
283 the Mozambique Channel in comparison with other coastal regions with a substantial river input



284 (Fig. 1f), where values can be as high as 65% (De Bar et al., 2016; Lattaud et al., 2017).  
285 Moreover, the BIT values are also relatively low at 0.01-0.42. Further confirmation of the low  
286 amount of terrestrial input in the analyzed surface sediments comes from the low C/N values  
287 (between 4.2 and 8.9 for the VA surface sediments; Schulz et al., 2011), characteristic of low  
288 terrestrial OM input (Meyers 1994). Nevertheless, the slightly higher values of both the BIT  
289 index and the  $F_{1,15-C32}$  near the river mouths indicate that both proxies do seem to trace present  
290 day riverine input into the Mozambique Channel, in line with earlier findings of other coastal  
291 margins influenced by river systems (De Bar et al., 2016; Lattaud et al., 2017).

292

#### 293 *4.2. Past variations in riverine input in the Mozambique Channel*

294 We compared the record of  $F_{1,15-C32}$  with previously published proxy records, in particular the  
295 BIT index (Kasper et al., 2015) and log (Ca/Ti) (van der Lubbe et al., 2016). These two proxies  
296 show the same pattern as  $F_{1,15-C32}$  (Fig. 2). Indeed, the BIT index and the percentage of  $C_{32}\ 1,15$ -  
297 diol are strongly correlated ( $r^2 = 0.83$ ,  $p < 0.001$ ). Since the #ring tetra of brGDGTs varies between  
298 0.06 and 0.4 (Fig. S1a) and is significantly negatively correlated with the BIT values, the brGDGTs  
299 are predominantly derived from the continent (cf. Sinninghe Damsté, 2016) and thus the BIT is  
300 likely reflecting terrigenous input in the marine environment. Furthermore, the percentage of  
301  $C_{32}\ 1,15$ -diol also shows a significant negative correlation with log(Ca/Ti) ( $r^2=0.43$ ,  $p < 0.0001$ ,  
302 van der Lubbe et al., 2016). This is another proxy for riverine input since Ti is mainly derived  
303 from erosion of continental rocks transported to the ocean through rivers, whereas Ca derives  
304 predominantly from the marine environment.



305 The records of  $F_{1,15-C32}$  and BIT index show three major variations: a steep drop from 19 to 10 ka,  
306 a slow increase from 38 to 21 ka during the Last Glacial Stage and a steep decrease between 40  
307 to 38 ka. The largest change in the BIT index and  $F_{1,15-C32}$  is between 19 to 10 ka, i.e. a major  
308 drop which coincides with an interval of rapid sea level rise (Fig. 2b). Following Menot et al.  
309 (2006), we explain the drop in the BIT index, and consequently also the drop in  $F_{1,15-C32}$ , by the  
310 significant sea level rise occurring during this period. Rising sea level flooded the Mozambique  
311 plateau, moving the river mouth further away from the core site and establishing more open-  
312 marine conditions. This most likely resulted in lower  $F_{1,15-C32}$  and BIT values, conditions that  
313 remained throughout the Holocene. The decrease in the delivery of terrestrial matter is also  
314 seen in element ratios (Fe/Ca) and organic proxies (BIT) in nearby core GeoB9307-3 (Schefuß et  
315 al., 2011), which is located closer to the present day river mouth in the Mozambique plateau  
316 (Fig. 1a). Likewise, the gradual increase in the BIT index and  $F_{1,15-C32}$  between 38 and 21 ka  
317 occurred at a time when sea-level was decreasing (Fig 2b., Grant et al., 2014; Rohling et al.,  
318 2014) and thus the river mouth came closer to our study site. Furthermore, between 38 and 35  
319 ka there is also an increase in precipitation in the catchment as reconstructed by the  $\delta D$  of  $n$ -  
320 alkanes in surrounding sediment cores (Tierney et al., 2008; Schefuß et al., 2011; Wang et al.,  
321 2013a; Fig. 2d). A wetter period may be characterized by increased erosion and a higher river  
322 flow, which could bring more C<sub>32</sub> 1,15-diols and brGDGTs into the marine realm. The decrease of  
323 BIT values and  $F_{1,15-C32}$  during 40-38 ka coincides with Heinrich event 4 (H4), a cold and dry event  
324 in this part of Africa (Partridge et al., 1997; Tierney et al., 2008; Thomas et al., 2009), with dry  
325 conditions perhaps leading to a reduced riverine input into the ocean and also a reduced input  
326 of brGDGTs and the C<sub>32</sub> 1,15-diol.



327 Interestingly, there are two periods where BIT and  $F_{1,15\text{-}C_{32}}$  records diverge (Fig. 2a): during the  
328 Younger Dryas (YD; 12.7–11.6 ka) and Heinrich event 1 (H1; 17–14.6 ka) with the BIT index  
329 decreasing ca. 1 ky later than  $F_{1,15\text{-}C_{32}}$ . Comparison with the Ca/Ti ratio shows that both during  
330 H1 and the YD, the Ca/Ti ratio increased at the same time as the  $C_{32}$  1,15-diol but earlier than  
331 the BIT index, suggesting that the latter was influenced by other parameters. The BIT index is  
332 the ratio of brGDGTs (produced mostly in soil or in-situ in rivers in our area based on the low  
333 values for #ring tetra; Sinninghe Damsté, 2016) over crenarchaeol (produced in marine or  
334 lacustrine environments; Schouten et al., 2013 and references cited therein). As both the Ti/Ca  
335 ratio and  $F_{1,15\text{-}C_{32}}$  indicate a decrease in riverine input, a constant BIT index can be explained by  
336 two options: a simultaneous decrease in crenarchaeol (marine) production or a change in soil  
337 input with higher brGDGT concentrations eroding into the river. The concentration of  
338 crenarchaeol during H1 is relatively stable but there is a slight decrease of crenarchaeol during  
339 YD (Fig. S2b). Thus, the difference between BIT and  $F_{1,15\text{-}C_{32}}$  during YD can be partly explained by  
340 decreased crenarchaeol production together with a decrease in branched GDGTs due to a  
341 reduced river input leading to relatively stable BIT values. In contrast, crenarchaeol and brGDGT  
342 concentrations are relatively stable during H1 and thus the lower river influx, as indicated by the  
343 Ca/Ti and  $F_{1,15\text{-}C_{32}}$ , apparently did not lead to a decrease in brGDGT input. This could be due to a  
344 shift of sources of soil which are eroded in the river, i.e. if in this period there is a shift towards  
345 soils with relatively higher brGDGT concentrations, the BIT index would remain high despite a  
346 decrease in riverine input.  
  
347 A shift in soil sources may be due to two major changes that happened during this period (and  
348 also during the YD), i.e. a shift in catchment area of the Zambezi River (Schefuß et al., 2011, Just



349 et al., 2014) and a shift in the relative influence of the Zambezi River versus northern  
350 Mozambique rivers (van der Lubbe et al., 2016). The shift in catchment area is evident from the  
351 higher influx of kaolinite-poor soil into the marine system during H1 and YD (Just et al., 2014)  
352 coming from the Cover Sands of the coastal Mozambique area (Fig. 3d, blue circle), relative to  
353 the kaolinite-rich soils of the hinterlands (Fig. 3d, red circles). If the brGDGT concentrations from  
354 the latter region are higher, then this change of soil input could lead to a stable brGDGT flux into  
355 the marine environment, despite decreasing Zambezi River runoff. Support for a shift in soil  
356 sources comes from the soil pH record reconstructed from brGDGTs, which during the YD shows  
357 a shift towards more acidic soils. However, no changes in soil pH are observed during H1.  
358 The relative influence of other rivers (Lurio, Rovuma Rivers) relative to the Zambezi River (Fig.  
359 3d green circle) was inferred from neodymium isotopes by Van der Lubbe et al. (2016), i.e. more  
360 radiogenic rocks are found in the northern river catchments in comparison to the rocks in the  
361 Zambezi catchment (Fig. 2b). These authors found that during H1 and YD, the relative  
362 contribution of the northern rivers is lower than normal, likely due to drought conditions north  
363 of the Zambezi catchment area (Tierney et al., 2008, 2011; Just et al., 2014). These northern  
364 rivers run through a catchment containing mainly humid highstand soils, which are different soil  
365 types than observed in the catchment area of the Zambezi River (van der Lubbe et al., 2016).  
366 Higher brGDGT concentrations in the soils of the catchment areas of the Zambezi River can  
367 potentially explain the discrepancy between BIT and  $F_{1,15-C32}$ , i.e. during H1 and YD there is more  
368 input of brGDGT-rich soils from the Zambezi than brGDGT-poor soils from the northern rivers  
369 leading to constant BIT values despite a dropping riverine input. Further research examining the



370 brGDGT contents of soils in the different river catchment areas is required to distinguish  
371 between the different hypotheses.

372 *4.3. Past variations in riverine input in the Eastern Mediterranean Sea*

373 Like with the Mozambique Channel core, we compared  $F_{1,15\text{-}C_{32}}$  in core GeoB7702 with other  
374 terrigenous proxies: BIT index, log (Ca/Ti) and strontium isotopes, the latter to infer the relative  
375 importance of the Blue Nile and the White Nile as source regions (Fig. 4c-e). The BIT values (data  
376 from Castañeda et al., 2010) shows a significant positive correlation with  $F_{1,15\text{-}C_{32}}$  ( $r^2=0.38$ ,  $p <$   
377 0.05), while log (Ca/Ti) shows a negative correlation to  $F_{1,15\text{-}C_{32}}$ , again in agreement with a  
378 terrigenous origin of the  $C_{32}$  1,15-diol.  $F_{1,15\text{-}C_{32}}$  and BIT records show much lower Holocene  
379 values compared to pre-Holocene (12±6% and 0.18±0.06 for the Holocene and 27±11% and  
380 0.38±0.11 before the Holocene, respectively), which again can be linked to the sea level rise  
381 occurring during the last deglaciation, i.e. our study site was further away from the river mouth  
382 and the amount of terrigenous OM reaching the site decreased. Both records show low values  
383 during H1 comparable to the Holocene. These low values can be attributed to enhanced aridity  
384 in the Nile River catchment (Castañeda et al., 2016) leading to lower river flow and decreasing  
385 the amount of terrigenous OM reaching our core site.

386 In this core, there are 3 major discrepancies observed between the BIT index and  $C_{32}$  1,15-diol:  
387 (1) during the LGM, between 22-19 ka, where the  $C_{32}$  1,15-diol shows a decrease while the BIT  
388 index remains constant, (2) during the onset of the deposition of S1 (6.1-10.5 ka, Grant et al.,  
389 2016) where the BIT index decreases later than the  $C_{32}$  1,15-diol, and (3) after 2 ka when the BIT  
390 index increases while the  $C_{32}$  1,15-diol decreases. For the LGM the percentage of  $C_{32}$  1,15-diol is



391 decreasing, log (Ca/Ti) is as well, but the BIT index remains constant indicating that there is no  
392 significant decrease in terrigenous OM reaching the core site at that time. There is no significant  
393 change in continental climate, based on the findings of Castañeda et al. (2016), suggesting no  
394 change in vegetation cover or river flux. This suggests that the change in  $F_{1,15-C_{32}}$  is not due to a  
395 change in the input of  $C_{32}$  1,15-diol but in other, mainly marine derived, diols, in particular the  
396  $C_{30}$  1,15-diol. An increase in this marine diol will lower the  $F_{1,15-C_{32}}$  but if the amount of  
397 crenarchaeol is not changing at the same time, the BIT values will remain unaffected.

398 The deposition of S1 is described as a period of increased riverine input leading to stratification  
399 and anoxia (Rossignol-Strick et al., 1982). However, an increased river input is neither reflected  
400 in the  $C_{32}$  1,15-diol nor in the BIT index, in fact both of them are asynchronously decreasing.  
401 Castañeda et al. (2010) showed that the decrease in the BIT index is due to a large increase in  
402 crenarchaeol (Fig. S3b), much larger than the increase in brGDGTs, due to increased productivity  
403 and preservation. A similar scenario may apply for the diols, i.e. the marine diols (in particular  
404 the  $C_{30}$  1,15-diol, data not shown) are also increasing at that time more substantially than the  
405  $C_{32}$  1,15-diol, thus lowering the percentage of  $C_{32}$  1,15-diol. However, there is a difference in  
406 timing, i.e. the BIT index decreases slightly later than the  $C_{32}$  1,15-diol (9.1 and 10.5 ka,  
407 respectively). The decrease in the  $C_{32}$  1,15-diol coincides with a substantial increase in sea level  
408 (Fig. 4b). This increase in sea level will increase the distance between the core site and the river  
409 mouth decreasing the amount of terrigenous material reaching the site. This decrease is also  
410 visible to some extent in the log (Ca/Ti) but not in the BIT index. Possibly, like with the  
411 Mozambique Channel, the brGDGT fluxes in the river was much higher at that time. Indeed, the  
412 Sr isotopes suggest a major shift from a Blue Nile to a White Nile source at this time, with the



413 latter possibly containing more eroded soils with high brGDGT concentrations. This shift in soil  
414 sources is also shown in the change towards more acidic soil pH during that period based on the  
415 CBT index (Fig. S1d).

416 For the most recent part of the record (0-5 ka), the BIT index increases, while the percentage of  
417  $C_{32}$  1,15-diol is slightly decreasing. Since  $\log(Ca/Ti)$  (Fig. 4c) is decreasing at this time, it suggests  
418 that river run off was decreasing leading to lower  $C_{32}$  1,15-diol input but apparently not to a  
419 change in the BIT index. The  $\delta D_{leafwaxes}$  (Fig 4.d) shows it was period of increased aridity which  
420 was probably the cause of the decreased runoff. The reason the BIT index is increasing rather  
421 than decreasing is due to an increase in brGDGT concentration (Fig. 3b), despite evidence for a  
422 decrease in river runoff. This can possibly be linked to the amount of vegetation in the Nile  
423 catchment, i.e. at that time there was a decrease in vegetation cover (Blanchet et al., 2014,  
424 Castañeda et al., 2016) which led to more soil erosion and thus potentially a higher brGDGT flux  
425 and a higher BIT index.

426 The results for the Nile core as well as those from the Mozambique Channel illustrate that the  
427  $C_{32}$  1,15-diol seems a suitable proxy for reconstructing past riverine input into coastal seas.  
428 However, our interpretation of the  $C_{32}$  1,15-diol record relies on the assumption that production  
429 of this diol in rivers is not changing with different hydroclimate fluctuations on land, something  
430 which needs to be tested. De Bar et al. (2016) showed that the percentage of  $C_{32}$  1,15-diol in the  
431 Tagus river in Portugal did not significantly change over the course of a year, suggesting that this  
432 assumption might be valid.

433 **6. Conclusion**



434 We studied core-tops in the Mozambique Channel and two sediment cores, in the Mozambique  
435 Channel, off the Zambezi River mouth and in the Eastern Mediterranean Sea, offshore the Nile  
436 delta, to test the percentage of C<sub>32</sub> 1,15 diol as a proxy for riverine input into the marine realm.  
437 The surface sediments show that the C<sub>32</sub> 1,15-diol traces present day riverine input into the  
438 Mozambique Channel, supported by the BIT index. In both sediment records, the C<sub>32</sub> 1,15-diol is  
439 significantly correlated with the BIT index showing the applicability of this proxy to trace riverine  
440 input, but also showed some discrepancies. This can be explained by the different terrestrial  
441 sources of these proxies, i.e. the BIT index is reflecting soil and riverine OM input and the C<sub>32</sub>  
442 1,15-diol is mainly reflecting riverine OM input. Our multiproxy approach shows that the timing  
443 of changes in the different terrestrial proxies records can differ due to changes in catchment  
444 area or to shifting importance of the different source rivers.

445 **Author contribution**

446 S. S. and J. L. designed the study. J. Lattaud analyzed the surface sediments for diols and GDGT and core  
447 GeoB 7702-3 for diols, I. C. sampled and extracted the surface sediments and the sediment cores  
448 64PE304-80 and GeoB 7702-3, D. D. analyzed the sediment core 64PE304-80 for diols. H. S. collected the  
449 VA core-tops. J. L., S. S., I. C. and J.S. S. interpreted the data. J. L. wrote the manuscript with input of all  
450 authors.

451 The authors declare that they have no conflict of interest.

452 **Acknowledgement**

453 We thanks Anchelique Mets and Jort Ossebaar for analytical help. This research has been  
454 funded by the European Research Council (ERC) under the European Union's Seventh



455 Framework Program (FP7/2007-2013) ERC grant agreement [339206] to S.S., J.S.S.D. and S.S.  
456 received financial support from the Netherlands Earth System Science Centre and this work was  
457 in part carried out under the program of the Netherlands Earth System Science Centre (NESSC),  
458 financially supported by the Ministry of Education, Culture and Science (OCW).

459

#### 460 **References**

461 Beilfuss, R. and Santos, D. : Patterns of hydrological change in the Zambezi delta. Mozambique  
462 (Working Paper No. 2, International Crane Foundation, Sofala, Mozambique, 2001), 1–89, 2001.

463 Blanchet, C.L., Frank, M. and Schouten, S. : Asynchronous changes in vegetation, runoff and  
464 erosion in the Nile River watershed during the Holocene, 2014, PLoS ONE 9(12): e115958.  
465 doi:10.1371/journal.pone.0115958.

466 Box, M.R., Krom, M.D., Cliff, R.A., Bar-Matthews, M., Almogi-Labin, A., Ayalon, A. and Pateme,  
467 M. : Response of the Nile and its catchment to millennial-scale climatic change since the LGM  
468 from Sr isotopes and major elements of East Mediterranean sediments, Quat. Sci. Rev., 30, 431–  
469 442, 2011. doi.org/10.1016/j.quascirev.2010.12.005.

470 Camberlin, P. : The Nile, chapter Nile basin climate, ed. Springer, 307–333, 2009.

471 Castañeda, I.S., Schefuß, E., Pätzold, J., Sinninghe Damsté, J.S., Weldeab, S. and Schouten, S. :  
472 Millennial-scale sea surface temperature changes in the eastern Mediterranean (Nile River Delta  
473 region) over the last 27,000 years, Paleoceanography, 25, 2010. doi:10.1029/2009PA001740.



- 474 Castañeda, I.S., Schouten, S., Pätzold, J., Lucassen, F., Kasemann, S., Kuhlmann, H. and Schefuß,  
475 E. : Hydroclimate variability in the Nile River Basin during the past 28,000 years, Earth Planet.  
476 Sci. Lett., 438, 47-56, 2016. doi.org/10.1016/j.epsl.2015.12.014.
- 477 Collister, J.W., Rieley, G., Stern, B., Eglinton, G. and Fry, B. : Compound-specific  $\delta^{13}\text{C}$  analyses of  
478 leaf lipids from plants with differing carbon dioxide metabolisms, Org. Geochem., 21 (6-7), 619-  
479 627, 1994. doi.org/10.1016/0146-6380(94)90008-6.
- 480 Cooke, M.P., Talbot, H.M. and Wagner, T. : Tracking soil organic carbon transport to continental  
481 margin sediments using soil-specific hopanoid biomarkers: A case study from the Congo fan  
482 (ODP site 1075), Org. Geochem., 39 (8), 965-971, 2008. doi.org/10.1016/j.orggeochem.
- 483 De Bar, M., Dorhout, D. J., C., Hopmans, E.C., Sinninghe Damsté, J.S. and Schouten, S. :  
484 Constraints on the application of long chain diol proxies in the Iberian Atlantic margin, Org.  
485 Geochem., 184-195, 2016. doi/10.1016/j.orggeochem.2016.09.005.
- 486 De Jonge, C., Stadnitskaia, A., Hopmans, E.C., Cherkashov, G., Fedotov, A., Streletskaya, I.D.,  
487 Vasiliev, A.A. and Sininghe Damsté, J.S. : Drastic changes in the distribution of branched  
488 tetraether lipids in suspended matter and sediments from the Yenisei River and Kara Sea  
489 (Siberia): Implications for the use of brGDGT-based proxies in coastal marine sediments,  
490 Geochimica et Cosmochimica Acta 165 200-225, 2015. doi.org/10.1016/j.gca.2015.05.044.
- 491 Eglinton, T.I. and Eglinton, G. : Molecular proxies for paleoclimatology, Earth Planet. Sc. Lett.,  
492 275, 1-16, 2008. doi/10.1016/j.epsl.2008.07.012.



- 493 Fallet, U., Brummer, G.-J., Zinke, J., Vogels, S. and Ridderinkhof, H. : Contrasting seasonal fluxes  
494 of planktonic foraminifera and impacts on paleothermometry in the Mozambique Channel  
495 upstream of the Agulhas Current, Paleoceanography, 25, 1525-2027, 2010.  
496 doi:10.1029/2010PA001942.
- 497 Fallet, U., Castañeda, I.S., Henry-Edwards, A., Richter, T.O., Boer, W., Schouten, S. and Brummer,  
498 G.-J. : Sedimentation and burial of organic and inorganic temperature proxies in the  
499 Mozambique Channel, SW Indian Ocean, Deep Sea Res. Pt1., 59, 37-53, 2012.  
500 doi:10.1016/j.dsr.2011.10.002.
- 501 Fekete, B. M., Vörösmarty, C. J. and Grabs, W. : Global, Composite runoff fields based on  
502 observed river discharge and simulated water balances, Global Biogeochem. Cycles, 16 (3), 15-  
503 1–15-10, 1999.
- 504 Foucault, A. and Stanley, D.J. : Late Quaternary paleoclimatic oscillations in East Africa recorded  
505 by heavy mineral in the Nile delta, Nature, 339, 44-46, 1989. doi:10.1038/339044a0.
- 506 Fry, B. and Sherr, E. B. :  $\delta^{13}\text{C}$  measurements as indicators of carbon flow in marine and  
507 freshwater ecosystems, Contributions to Marine Science 27, 13-47, 1984. doi:10.1007/978-1-  
508 4612-3498-2\_12.
- 509 Gimeno, L., Drumond, A., Nieto, R., Trigo, R.M. and Stohl, A. : On the origin of continental  
510 precipitation, Geophys. Res. Lett., 37, 2010. doi: 10.1029/2010GL043712.



511 Goñi, M.A., Ruttenberg, K.C. and Eglington, T.I. : Sources and contribution of terrigenous organic  
512 carbon to surface sediments in the Gulf of Mexico, Nature, 389, 275-278, 1997.

513 doi:10.1038/38477.

514 Grant, K.M., Rohling, E.J., Ramsey, C.B., Cheng, H., Edwards, R.L., Florindo, F., Heslop, D., Marra,  
515 F., Roberts, A.P., Tamisiea, M.E. and Williams, F. : Sea-level variability over five glacial cycles,  
516 Nature com., 5, 2014. doi: 10.1038/ncomms6076.

517 Hedges, J. I., Clark, W. A., Quay, P. D., Richey, J. E., Devol, A. H. and Santos, U. M. : Composition  
518 and fluxes of particulate organic material in the Amazon River, Limnology and Oceanography.  
519 31, 717-738, 1986. doi: 10.4319/lo.1986.31.4.0717.

520 Hedges, J. I. and Oades, J. M. : Comparative organic geochemistries of soils and sediments,  
521 Organic Geochemistry. 27, 319–361, 1997. doi.org/10.1016/S0146-6380(97)00056-9.

522 Hopmans, E.C., Weijers, J.W.H., Schefuß, E., Herfort, L., Sinninghe Damsté, J.S. and Schouten, S. :  
523 A novel proxy for terrestrial organic matter in sediments based on branched and isoprenoid  
524 tetraether lipids, Earth Planet. Sc. Lett., 224 (1-2), 107-116, 2004.  
525 doi.org/10.1016/j.epsl.2004.05.012.

526 Hopmans, E.C., Schouten, S. and Sinninghe Damsté, J.S. : The effect of improved  
527 chromatography on GDGT-based palaeoproxies, Org. Geochem., 93, 1-6, 2016.  
528 doi.org/10.1016/j.orggeochem.2015.12.006.



- 529 Just, J., Schefuß, E., Kuhlmann, H., Stuut, J.-B. W. and Pätzold, J. : Climate induced sub-basin
- 530 source-area shifts of Zambezi River sediments over the past 17 ka, *Palaeogeogr., Palaeocl.*, 410,
- 531 190-199, 2014. doi.org/10.1016/j.palaeo.2014.05.045.
- 532 Kasper, S., van der Meer, M.T.J., Castañeda, I.S., Tjallingii, R., Brummer, G.-J. A., Sinninghe
- 533 Damsté, J.S. and Schouten, S. : Testing the alkenone D/H ratio as a paleo indicator of sea surface
- 534 salinity in a coastal ocean margin (Mozambique Channel), *Org. Geochem.*, 78, 62-68, 2015.
- 535 doi.org/10.1016/j.orggeochem.2014.10.011.
- 536 Krom, M.D., Stanley, J.-D., Cliff, R. A., Woodward, J.C. : Nile River sediment fluctuations over the
- 537 past 7000 yr and their key role in sapropel development, *Geology*, 30, 71-74, 2002. doi:
- 538 10.1130/0091-7613(2002)030<0071.
- 539 Lattaud, J., Kim, J.-H., De Jonge, C., Zell, C., Sinninghe Damsté, J.S. and Schouten, S. : The C<sub>32</sub>
- 540 alkane-1,15-diol as a tracer for riverine input in coastal seas, *Geochim. Cosmochim. Ac.*, 202C,
- 541 146-158, 2017. doi.org/10.1016/j.gca.2016.12.030.
- 542 Ménot, G., Bard, E., Rostek, F., Weijers, J.W.H., Hopmans, E.C., Schouten, S. and Sinninghe
- 543 Damsté, J.S. : Early reactivation of European Rivers during the last deglaciation, *Science*, 313,
- 544 1623-1625, 2006. doi: 10.1126/science.1130511.
- 545 Meyers, P. A. : Preservation of elemental and isotopic source identification of sedimentary
- 546 organic matter, *Chem. Geol.* 114, 289-302, 1994. doi.org/10.1016/0009-2541(94)90059-0.
- 547 Nehama, F.P.J. and Reason, C.J.C. : Morphology of the Zambezi River Plume on the Sofala Bank,
- 548 Mozambique Western Indian Ocean, *J. Mar. Sci.* 13, 1-10, 2014.



- 549 Nicholson, S.E. : A revised picture of the structure of the “monsoon” and land ITCZ over West  
550 Africa, *Clim. Dynam.*, 32, 1155–1171-, 2009. doi: 10.1007/s00382-008-0514-3.
- 551 Partridge, T.C., Demenocal, P.B., Lorentz, S.A., Paiker, M.J. and Vogel, J.C. : Orbital forcing of  
552 climate over south Africa: A 200,000-year rainfall record from the Pretoria saltpan, *Quat. Sc.*  
553 *Rev.*, 16, 1125–1133, 1997. doi:10.1016/S0277-3791(97)00005-X.
- 554 Peterse, F., van der Meer, J., Schouten, S., Weijers, J.W.H., Fierer, N., Jackson, R.B., Kim, J.-H.  
555 and Sinninghe Damste, J.S. : Revised calibration of the MBT–CBT paleotemperature proxy based  
556 on branched tetraether membrane lipids in surface soils, *Geochim. Cosmochim. Acta.*, 96, 215–  
557 229, 2012. doi:10.1016/j.gca.2012.08.011.
- 558 Ponton, C., West, A., Feakins, S.J. and Valier G. : Leaf wax biomarkers in transit record river  
559 catchment composition, *Geophys. Res. Lett.*, 41, 6420–6427, 2014.
- 560 Rampen, S.W., Schouten, S., Wakeham, S.G. and Sinninghe Damsté, J.S. : Seasonal and spatial  
561 variation in the sources and fluxes of long chain diols and mid-chain hydroxy methyl alkanoates  
562 in the Arabian Sea, *Org. Geochem.*, 38, 165–179, 2007.  
563 doi.org/10.1016/j.orggeochem.2006.10.008.
- 564 Rampen, S.W., Willmott, V., Kim, J.-H., Uliana, E., Mollenhauer, G., Schefuß, E., Sinninghe  
565 Damsté, J.S. and Schouten, S. : Long chain 1,13- and 1,15-diols as a potential proxy for  
566 palaeotemperature reconstruction, *Geochim. Cosmochim. Acta* 84, 204–216, 2012.  
567 doi.org/10.1016/j.gca.2012.01.024.



- 568 Rampen, S.W., Datema, M., Rodrigo-Gámiza, M., Schouten, S., Reichart, G.-J. and Sinninghe
- 569 Damsté, J.S. : Sources and proxy potential of long chain alkyl diols in lacustrine environments,
- 570 Geochimi. Cosmochimi. Acta, 144, 59-71, 2014. doi.org/10.1016/j.gca.2014.08.033.
- 571 Rohling, E.J., Foster, G.L., Marino, G., Roberts, A.P., Tamisiea, M.E. and Williams, F. : Sea-level
- 572 and deep-sea-temperature variability over the past 5.3 million years, Nature, 508, 477-482,
- 573 2014. doi:10.1038/nature13230.
- 574 Rommerskirchen, F., Plader, A., Eglinton, G., Chikaraishi, Y. and Rullkötter, J. : Chemotaxonomic
- 575 significance of distribution and stable carbon isotopic composition of long-chain alkanes and
- 576 alkan-1-ols in C<sub>4</sub> grass waxes, Org. Geochem., 37, 1303–1332, 2006.
- 577 doi.org/10.1016/j.orggeochem.2005.12.013.
- 578 Ronco, P., Fasolato, G., and Di Silvio, G. : The case of Zambezi River in Mozambique: some
- 579 investigations on solid transport phenomena downstream Cahora Bassa Dam, Proceeding of
- 580 International Conference on Fluvial Hydraulics, Riverflow, 1345-1354, 2006. doi:
- 581 10.1201/9781439833865.ch143.
- 582 Rossignol-Strick, M., Nesteroff, W., Olive, P. and Vergnaud-Grazzini, C. : After the deluge:
- 583 Mediterranean stagnation and sapropel formation, Nature, 295, 105–110, 1982. doi:
- 584 10.1038/295105a0.
- 585 Schefuß, E., Kuhlmann, H., Mollenhauer, G., Prange, M. and Pätzold, J. : Forcing of wet phases in
- 586 southeast Africa over the past 17,000 years, Nature 480, 509-512, 2011.
- 587 doi:10.1038/nature10685.



- 588 Schlesinger, L.H. and Melack, J.M. : Transport of organic carbon in the world's rivers Tellus 33 (2)
- 589 172-187, 1981. doi.org/10.3402/tellusa.v33i2.10706.
- 590 Schouten, S., Hopmans, E.C. and Sinninghe Damsté, J.S.S., The organic geochemistry of glycerol
- 591 dialkyl glycerol tetraether lipids: A review, Org. Geochem., 54, 19-61, 2013.
- 592 doi.org/10.1016/j.orggeochem.2012.09.006.
- 593 Schulz, H., Lückge, A., Emeis, K.-C. and Mackensen, A. : Variability of Holocene to Late
- 594 Pleistocene Zambezi riverine sedimentation at the upper slope off the Mozambique, 15-21°S,
- 595 Mar. Geol., 286, 21-34, 2011. doi:10.1016/j.margeo.2011.05.003.
- 596 Sinninghe Damsté, J.S., Schouten, S., Hopmans, E.C., van Duin, A.C.T. and Geeenevasen, J.A.J.,
- 597 Crenarchaeol the characteristic core glycerol dibiphytanyl glycerol tetraether membrane lipid of
- 598 cosmopolitan pelagic crenarchaeota, Jour. Lip. Res., 43, 1641-1651, 2002. doi:
- 599 10.1194/jlr.M200148-JLR200.
- 600 Sinninghe Damsté, J.S. : Spatial heterogeneity of sources of branched tetraethers in shelf
- 601 systems: The geochemistry of tetraethers in the Berau River delta (Kalimantan, Indonesia),
- 602 Geochim. Cosmochim. Acta. 186, 13-31, 2016. doi.org/10.1016/j.gca.2016.04.033.
- 603 Smith, R.W., Bianchi, T.S. and Li, X. : A re-evaluation of the use of branched GDGTs as terrestrial
- 604 biomarkers: Implications for the BIT Index, Geochim. Cosmochim. Acta, 80, 14-29, 2012.
- 605 doi.org/10.1016/j.gca.2011.11.025.



- 606 Thomas, D.S.G., Bailey, R., Shaw, P.A., Durcan, J.A. and Singarayer, J.S. : Late Quaternary  
607 highstands at Lake Chilwa, Malawi: Frequency, timing and possible forcing mechanisms in the  
608 last 44 ka, Quat. Sc. Rev., 28, 526–539, 2009. doi:10.1016/j.quascirev.2008.10.023.
- 609 Tierney, J. E., Russell J.M., Huang, Y., Sininghe Damsté, J.S., Hopmans, E.C. and Cohen, A.S. :  
610 Northern Hemisphere controls on tropical southeast African climate during the past 60,000  
611 years, Science 322, 252–255, 2008. doi: 10.1126/science.1160485.
- 612 Tierney, J.E., Russell, J.M., Sininghe Damsté, J.S., Huang, Y. and Verschuren, D. : Late  
613 Quaternary behavior of the East African monsoon and the importance of the Congo Air  
614 Boundary, Quat. Sc. Rev. 30, 798–807, 2011. doi.org/10.1016/j.quascirev.2011.01.017
- 615 van der Lubbe, J. J. L., Tjallingii, R., Prins, M. A., Brummer, G.-J. A., Jung, S. J. A., Kroon, D. and  
616 Schneider, R. R. : Sedimentation patterns off the Zambezi River over the last 20,000 years, Mar.  
617 Geol., 355, 189–201, 2014. doi:10.1016/j.margeo.2014.05.0120025-3227.
- 618 van der Lubbe, J.J.L., Frank, M., Tjallingii, R. and Schneider, R. : Neodymium isotope constraints  
619 on provenance, dispersal, and climate-driven supply of Zambezi sediments along the  
620 Mozambique Margin during the past ~45,000 years, Geochem. Geophys., 17 (1), 181–198, 2016.  
621 doi:10.1002/2015GC006080.
- 622 Versteegh, G.J.M., Bosch, H.J. and De Leeuw, J.W. : Potential palaeoenvironmental information  
623 of C<sub>24</sub> to C<sub>36</sub> mid-chain diols, keto-ols and mid-chain hydroxy fatty acids; a critical review, Org.  
624 Geochem., 27, 1–13, 1997. doi.org/10.1016/S0146-6380(97)00063-6.



- 625 Versteegh, G.J.M., Jansen, J.H.F., De Leeuw, J.W. and Schneider, R.R. : Mid-chain diols and keto-  
626 ols in SE Atlantic sediments: a new tool for tracing past sea surface water masses?, Geochim.  
627 Cosmochim. Ac. 64, 1879–1892, 2000. doi.org/10.1016/S0016-7037(99)00398-1.
- 628 Villanueva, L., Besseling, M., Rodrigo-Gámiz, M., Rampen, S.W., Verschuren, D. and Sinninghe  
629 Damsté, J.S. : Potential biological sources of long chain alkyl diols in a lacustrine system, Org.  
630 Geochem., 68, 27–30, 2014. doi.org/10.1016/j.orggeochem.2014.01.001.
- 631 Volkman, J.K., Barnett, S.M. and Blackburn, S.I. : Eustigmatophyte microalgae are potential  
632 sources of C<sub>29</sub> sterols, C<sub>22</sub>–C<sub>28</sub>n-alcohols and C<sub>28</sub>–C<sub>32</sub>n-alkyl diols in freshwater environments,  
633 Org. Geochem., 30, 307–318, 1999. doi.org/10.1016/S0146-6380(99)00009-1.
- 634 Walford, H.L., White, N.J. and Sydow, J.C. : Solid sediment load history of the Zambezi Delta,  
635 Earth Planet. Sc. Lett., 238 (1-2), 49-63, 2005. doi.org/10.1016/j.epsl.2005.07.014.
- 636 Wang, Y.V., Larsen, T., Leduc, G., Andersen, N., Blanz, T. and Schneider, R.R. : What does leaf  
637 wax δD from a mixed C<sub>3</sub>/C<sub>4</sub> vegetation region tell us?, Geochim. Cosmochim. Ac., 111, 128-129,  
638 2013. doi:10.1016/j.gca.2012.10.016.
- 639 Weijers, J.W.H., Schouten, S., van den Donker, J.C., Hopmans, E.C. and Sinninghe Damsté, J.S. :  
640 Environmental controls on bacterial tetraether membrane lipid distribution in soils, Geochim.  
641 Cosmochim. Ac., 71 pp. 703–713, 2007.
- 642 Weijers, J.W.H., Panoto, E., van Bleijswijk, J., Schouten, S., Rijpstra, W.I.C., Balk, M., Stams,  
643 A.J.M. and Sinninghe Damsté, J.S. : Constraints on the biological source(s) of the orphan



- 644 branched tetraether membrane lipids, Geomicrobiol J., 26 402–414, 2009.  
645 doi.org/10.1080/01490450902937293.
- 646 Weldeab, S., Emeis, K.-C., Hemleben, C. and Siebel, W. : Provenance of lithogenic surface  
647 sediments and pathways of riverine suspended matter in the Eastern Mediterranean Sea:  
648 evidence from  $^{143}\text{Nd}/^{144}\text{Nd}$  and  $^{87}\text{Sr}/^{88}\text{Sr}$  ratios, Chem. Geol., 186, 139-149, 2002.  
649 doi.org/10.1016/S0009-2541(01)00415-6.
- 650 Zell, C., Kim, J.-H., Dorhout, D., Baas, M. and Sinninghe Damsté, J.S.S., Sources and distributions  
651 of branched tetraether lipids and crenarchaeol along the Portuguese continental margin:  
652 Implications for the BIT index, Cont. Shelf Res., 96, 34-44, 2015.  
653 doi.org/10.1016/j.csr.2015.01.006.
- 654



655    **Figure Legend**

656    **Figure 1.** Map presenting (a) the location of the core-tops (LOCO transect in orange, VA core-  
657    tops in blue) and cores (stars), (b) the mean annual salinity, from NOAA 1x1° grid  
658    (<http://iridl.ldeo.columbia.edu>), (c) the BIT index (LOCO transect values, VA core-tops from this  
659    study), (d) the percentage of C<sub>32</sub> 1,15-diol in the core-tops, (e) #ring tetra of the surface  
660    sediments (#ring tetra as defined by Sinnenhe Damsté 2016), (f) Ternary diagram of C<sub>28</sub> (sum of  
661    C<sub>28</sub> 1,13 and C<sub>28</sub> 1,14), C<sub>30</sub> (sum of C<sub>30</sub> 1,13, C<sub>30</sub> 1,14 and C<sub>30</sub> 1,15) and C<sub>32</sub> (C<sub>32</sub> 1,15) diols (LOCO  
662    transect in orange, VA core-tops in blue, data from Lattaud et al. 2017 in purple). The maps have  
663    been draw using Ocean Data View.

664    **Figure 2.** Organic and lithologic proxy records for core 64PE304-80 and parallel core GIK16160-  
665    3. (a) BIT index indicating soil and riverine input (Kasper et al., 2015) and percentage of C<sub>32</sub> 1,15-  
666    diol tracing riverine input (b) Red Sea Level changes (Grant et al., 2013) (c) log(Ca/Ti) indicating  
667    terrestrial input (van der Lubbe et al., 2013), (d) reconstruction of δD precipitation based on leaf  
668    wax n-C<sub>29</sub> alkane of core GIK16160-3 (Wang et al., 2013), € ε<sub>Nd</sub> signatures of the clay fraction  
669    document changes in riverine influence (van der Lubbe et al., 2016). The grey bars show the  
670    Younger Dryas (YD) and Heinrich event 1 (H1) and 4 (H4).

671    **Figure 3.** Sources of riverine input in both area, (a) Location of core GeoB7702-3 (b) Close up  
672    location of core GeoB7702-3 and core 9509 (Box et al., 2011) (c) source of the Nile river  
673    sediments, Blue Nile: BN, White Nile: WN, Lake Tana: LT, Lake Victoria: LV (from Castañeda et  
674    al., 2016) and (d) the Mozambique Channel (red circles shows source areas of the Zambezi river  
675    during dry conditions, blue circle shows source area of the Zambezi river during wet conditions

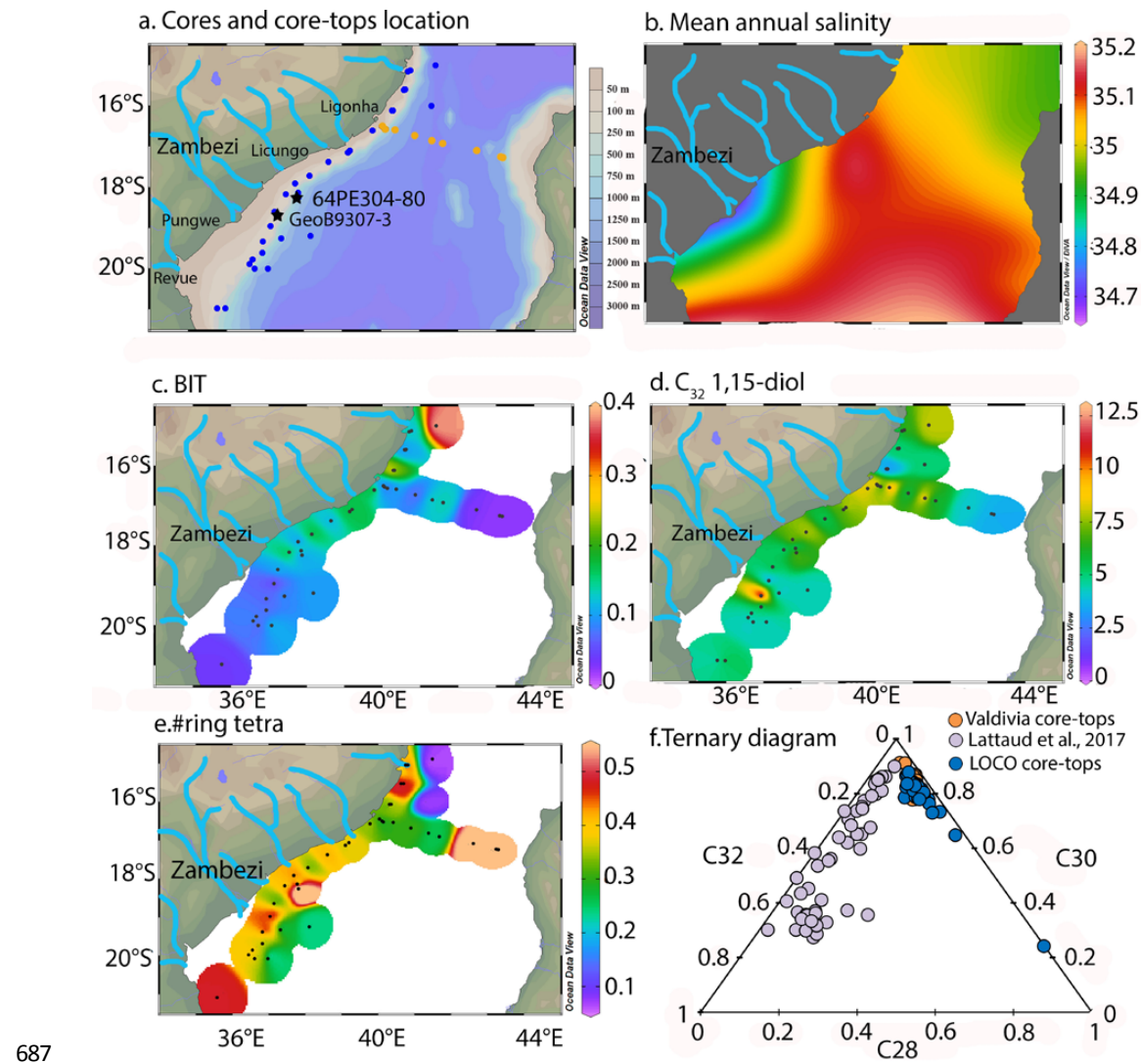


676 (Just et al., 2014), and green circle show northern rivers source area (van der Lubbe et al.,

677 2016)).

678 **Figure 4.** Organic and lithologic proxy records for core GeoB7702-3 and core 9509. (a) BIT index  
679 indicating soil and riverine input (Castañeda et al., 2010) and percentage of C<sub>32</sub> 1,15-diol tracing  
680 riverine input (b) Red Sea Level changes (Grant et al., 2013) (c) log(Ca/Ti) indicating terrestrial  
681 input (Castañeda et al., 2016), (d) reconstruction of δD precipitation based on leaf wax n-C<sub>31</sub>  
682 alkane (Castañeda et al., 2016), (e) <sup>87</sup>Sr/<sup>88</sup>Sr signatures of the sediment core 9509 (offshore the  
683 Israeli coast) document changes in riverine influence (Box et al., 2011). The grey bars show the  
684 sapropel layer (S1), Younger Dryas (YD), Heinrich event 1 (H1) and the Last Glacial Maximum  
685 (LGM).

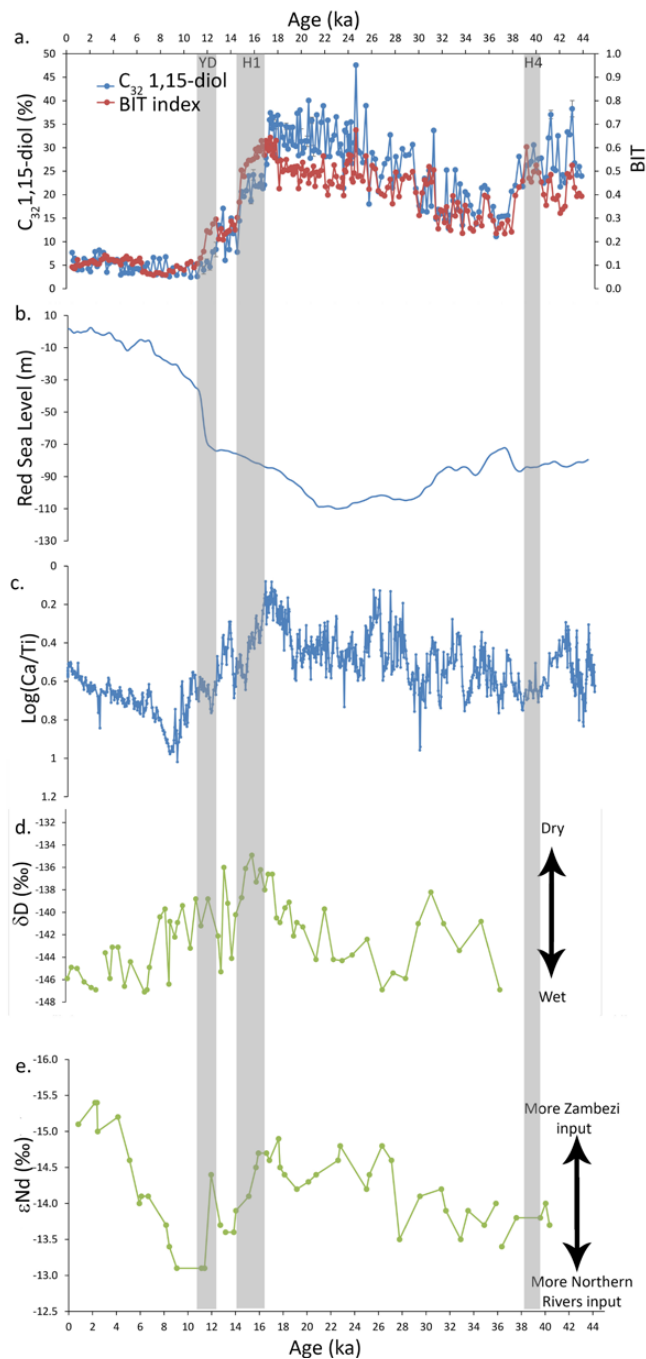
686



687

688 Figure 1

689



712 Figure 2

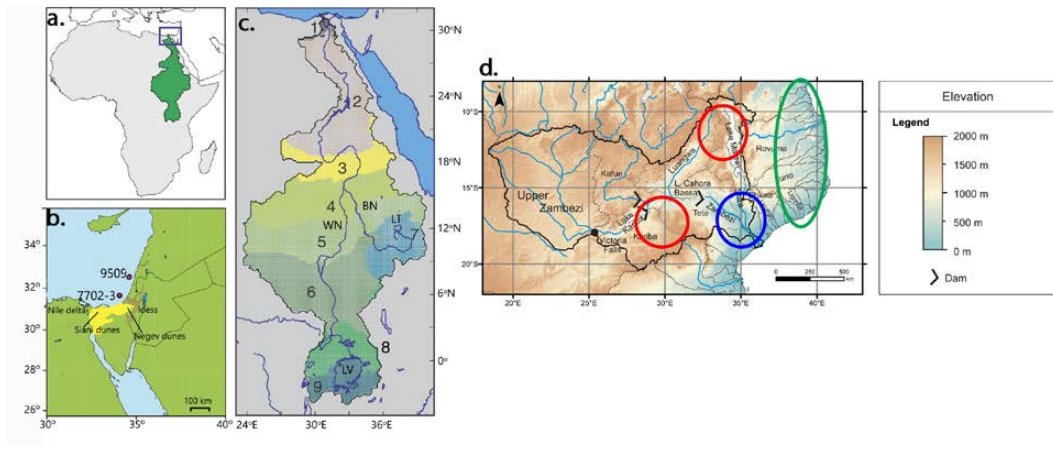


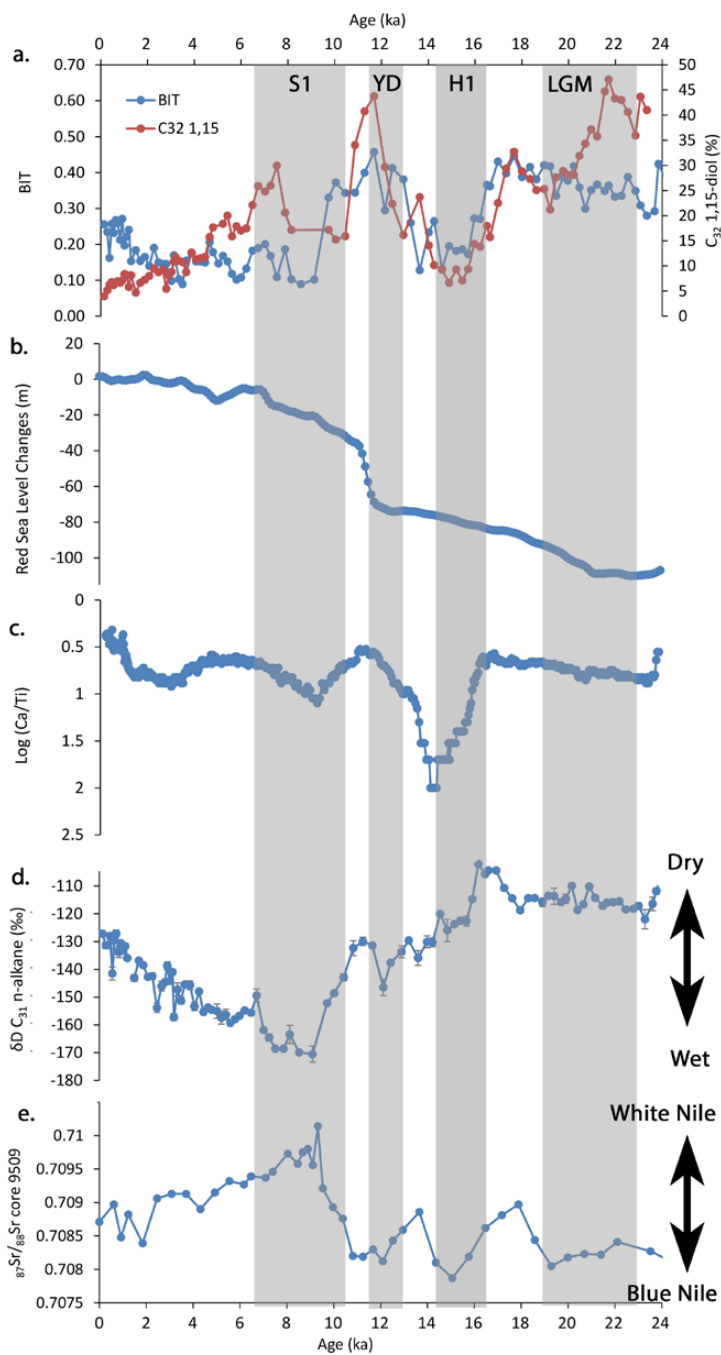
714

715

716 Figure 3

717





718

719 Figure 4